Journal of
Mechanics of
Materials and Structures

MULTISCALE ANALYSIS OF NANOSCALE THIN FILM CONSIDERING SURFACE EFFECTS: THERMOMECHANICAL PROPERTIES

Jinbok Choi, Maenghyo Cho and Wonbae Kim

Volume 5, № 1 January 2010

mathematical sciences publishers

JOURNAL OF MECHANICS OF MATERIALS AND STRUCTURES
Vol. 5, No. 1, 2010

MULTISCALE ANALYSIS OF NANOSCALE THIN FILM CONSIDERING SURFACE EFFECTS: THERMOMECHANICAL PROPERTIES

JINBOK CHOI, MAENGHYO CHO AND WONBAE KIM

The classical model for a thin film, based on continuum theory, is independent of size, and ignores surface effects. But the surface-to-bulk ratio becomes very large in small-scale structures such as nanofilms, nanowires, and nanobeams, and surface effects play an important role. Molecular dynamics simulation has been a conventional way to analyze these ultrathin structures, but structures in the range between submicro and micro are difficult to analyze by molecular dynamics simulation due to the restrictions of computing resources and time. In the present study, a continuum-based, size-dependent model is developed for predicting the thermomechanical properties of nanoscale structures, especially thin films. The proposed continuum-based thin plate finite element is efficient and reliable for the prediction of nanoscale film behavior.

1. Introduction

As the applications of nanosized structures such as thin films, nanobeams, and nanowires have increased in the field of electromechanical systems, the analysis of the physical and thermomechanical properties of these structures has been an issue in the design of these devices and the prediction of their performance.

The properties of nanosized structures can differ sharply from the bulk properties of the same material [Dingreville et al. 2005; Shenoy 2005], because surface effects, which are negligible in macrosized materials, play a dominant role as the surface-to-volume ratio becomes larger. These phenomena have been investigated in previous works with both experiments and molecular dynamics (MD) simulations. Cuenot et al. [2004] studied the surface tension effect on the mechanical properties of nanomaterials with electrostatic resonant-contact atomic force microscopy. The elastic properties of a silicon nanocantilever were calculated via molecular dynamics techniques, and it was shown that the elastic modulus decreases as the thickness of the specimen decreases [Park et al. 2005]. Miller and Shenoy [2000] and Cammarata and Sieradzki [1989] demonstrated that this size dependence arises due to the increasing importance that surfaces play as structures become smaller. It was shown by Cammarata [1994] that for a solid with one or more dimensions under 10 nm, the surface stress could be a principal factor in determining behavior. It was also shown that several kinetic and thermodynamic properties of thin polymer film could be changed by decreasing the film thickness, due to the surface and interface effects [Lang et al. 2006]. The elastic properties of ZnO nanofilms with different film thicknesses, surface orientations, and loading directions were investigated in Cao and Chen [2008] using molecular mechanics. Song and Huang [2009] studied

Keywords: surface effects, thin film, multiscale analysis, continuum, finite element method.
This work was supported by the Korea Science and Engineering Foundation (KOSEF) through the National Research Laboratory Program funded by the Korean government (MOST) (ROA-2009-000-20109-0). It was also supported by a WCU (World Class University) program through the Korea Research Foundation funded by the Ministry of Education, Science, and Technology (R31-2009-000-10083-0).

the effects of surface stress on bending behavior of nanowires with incremental deformation theory and a high-order continuum model was developed by Song et al. [2010] to study wave propagation in nanowires with surface effects. Some other researchers also considered size-dependent elasticity of nanowires due to nonlinearity [Liang et al. 2005; Park and Klein 2008]. But in this study we are focusing on prediction of the thermoelastic properties of thin film structures under the assumption of linear elasticity considering small deformation and temperature change.

Recently, it has become possible to simulate these nanosized structures with MD simulations because of the improvement in their numerical techniques and today's computing power, but it is still difficult to simulate structures in the range between the submicro and microscale due to restrictions of computing resources and time. MD simulations are still limited to problems of several million atoms for just a few nanoseconds. But it is often necessary to repeatedly analyze such structures to get an optimized design in practical applications. It is not efficient to apply the classical MD simulations to these problems. Therefore, continuum methods are appropriate for these problems where it is not tractable to apply the classical MD simulation. There have been several approaches to analyzing nanostructures based on continuum theories. Gao et al. [2006] suggested a finite element model to describe the size-dependent mechanical properties of nanostructures but did not try to obtain the surface elastic constants, and temperature effects were not considered in their formulation. An energy-based continuum model for the analysis of nanostructures was developed by Park et al. [2006] by adopting theories utilized in the Cauchy–Born rules. They also decomposed the total potential energy of the system into a bulk energy component and a surface energy component, but define the strain energy in terms of a relatively simple pair potential.

In the present study, the continuum-based method is considered to predict the overall thermomechanical properties of nanoscale structures. A general model for elastically isotropic solids with surface stress was suggested by [Gurtin and Murdoch 1975a; 1975b; 1978]. This model was adopted recently by some authors to analyze the elastic responses of nanoscale thin films [Lim and He 2004; Lu et al. 2006]. We especially focus on the investigation of the thermomechanical properties in thin film with a thickness ranging from a few nanometers to several tens of nanometers, and the finite element method (FEM) for the thin film structure is also implemented based on the continuum model. The proposed continuum-based thin film FEM is efficient and reliable for the prediction of nanoscale film behavior. Basically, the governing equations of this continuum model are based on the modified Kirchhoff plate theory, including surface effects [Lim and He 2004; Lu et al. 2006]. These equations can describe the dominant surface effects as the thickness of the thin film becomes very small [Miller and Shenoy 2000]. The conventional thin plate continuum model does not contain the surface energy term because this effect is negligibly small in the macroscale, as mentioned above; however, the surface energy needs to be considered in these nanosized structures. The present continuum model considering the size effect needs three surface parameters to represent the surface effects of the thin film. In this study, the necessary surface parameters are obtained from the MD simulations. Reliable and accurate surface parameters are essential for guaranteeing the accuracy of the solution of the continuum-based thin film FEM.

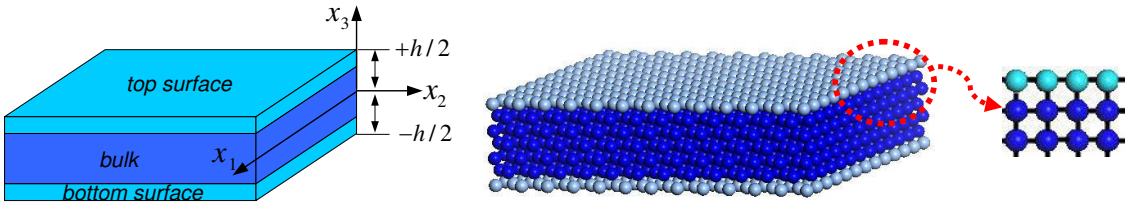

(a) (b)

Figure 1. Thin film structures for the continuum model (a) and atomistic structure of thin film (b): the alignments of bond chains of an atom in the surface and bulk are different.

2. Equilibrium equation of the thin film considering surface effects

Kirchhoff plate theory considering surface effects. For a thin film structure with a very small length scale in the thickness direction, a midplane, along with top and bottom surface layers of S^+ and S^- at $x_3 = \pm h/2$, can be defined, as shown in Figure 1a. In the figure the top and bottom surfaces are shown with finite thickness, to stress that additional surface energy has to be added to the classical Kirchhoff thin plate theory in order to consider the surface effects, but in fact, the surface layers do not have thickness in our continuum model.

The reason we consider the surface and bulk energy separately is that the atoms in the surface layers have fewer neighbors and consequently excess energy over atoms in the bulk (see Figure 1b). This energy difference results in unique and interesting properties of nanosized thin film structures.

In Kirchhoff thin plate theory, the displacement fields of the bulk layer are defined as

$$u_\alpha = u_\alpha^0 - x_3 u_{3,\alpha}^0, \qquad u_3 = u_3^0. \tag{1}$$

The displacements of the top and bottom surface layers (s^+, s^-) are u_α^{S+}, u_α^{S-}, u_3^{S+}, and u_3^{S-}. The displacement continuity conditions at the interface between the interior layer and surface layers can be represented as

$$\begin{aligned} u_\alpha^{s-} &= u_\alpha\big|_{x_3=-h/2} = (u_\alpha^o - x_3 w_{,\alpha})\big|_{x_3=-h/2} = u_\alpha^o + \frac{h}{2} w_{,\alpha}, \qquad u_3^{s+} = w, \\ u_\alpha^{s+} &= u_\alpha\big|_{x_3=h/2} = (u_\alpha^o - x_3 w_{,\alpha})\big|_{x_3=h/2} = u_\alpha^o - \frac{h}{2} w_{,\alpha}, \qquad u_3^{s-} = w. \end{aligned} \tag{2}$$

Temperature effects are considered in this study, so the temperature field is assumed to be linear through the thickness as $\Delta T(x_1, x_2) = \Delta T_1 + x_3 \Delta T_2$. The temperature change of the upper (ΔT^+) and lower (ΔT^-) surfaces of the thin film are given in the following form, respectively:

$$\Delta T^+ = \Delta T_1 + \frac{h}{2}\Delta T_2, \qquad \Delta T^- = \Delta T_1 - \frac{h}{2}\Delta T_2. \tag{3}$$

The virtual work principle is adopted to derive the governing equation of the thin film including the surface energy contribution. The total virtual work is given in the following form for a static problem: $\delta\Pi = \delta U - \delta W_E$, where δU is the variation of the internal strain energy, and the variation of the external

virtual work is given as

$$\delta W_E = \int_\Omega p_\alpha\, \delta u_\alpha^0 + p_3\, \delta w\, dA, \qquad \text{where } dA = dx_1\, dx_2, \tag{4}$$

where p_α is the tangential force intensity per unit area on the reference surface and p_3 is the transversal force intensity to the reference surface. The variation of the internal strain energy (δU) consists of the bulk energy and surface energy variations: $\delta U = \delta U_{\text{bulk}} + \delta U_{\text{surf}}$. The internal virtual bulk energy of the plate under the Kirchhoff assumption is written as

$$\begin{aligned}
\delta U_{\text{bulk}} &= \int_v \sigma_{ij}\, \delta\varepsilon_{ij}\, dv = \int_\Omega \int_{-h/2}^{h/2} \sigma_{\alpha\beta}(\delta\varepsilon_{\alpha\beta}^0 - x_3\, \delta w_{,\alpha\beta})\, dx_3 dA \\
&= \int_\Omega \int_{-h/2}^{h/2} \sigma_{\alpha\beta} \frac{1}{2}(\delta u_{\alpha,\beta}^0 + \delta u_{\beta,\alpha}^0) - \sigma_{\alpha\beta} x_3\, \delta w_{,\alpha\beta}\; dx_3 dA \\
&= \int N_{\alpha\beta}\, \delta u_{\alpha,\beta}^0 - M_{\alpha\beta}\, \delta w_{,\alpha\beta}\; dA, \qquad \text{where } \int_{-h/2}^{h/2} (\sigma_{\alpha\beta}, \sigma_{\alpha\beta} x_3)\, dx_3 = (N_{\alpha\beta}, M_{\alpha\beta}).
\end{aligned} \tag{5}$$

The surface internal virtual energy is expressed by

$$\delta U_{\text{surf}} = \int_{\Omega^+} \tau_{\alpha\beta}^+\, \delta\varepsilon_{\alpha\beta}^{s+} + \tau_{\alpha 3}^+\, \delta\gamma_{\alpha 3}^{s+} dA + \int_{\Omega^+} \tau_{\alpha\beta}^-\, \delta\varepsilon_{\alpha\beta}^{s-} + \tau_{\alpha 3}^-\, \delta\gamma_{\alpha 3}^{s-}\, dA. \tag{6}$$

Using the strain-displacement relationship in the surface, the surface internal virtual work can be written as

$$\begin{aligned}
\delta U_{\text{surf}} &= \int_{\Omega^+} \tau_{\alpha\beta}^+\, \delta\varepsilon_{\alpha\beta}^{s+} + \tau_{\alpha 3}^+ \delta(u_{\alpha,3}^{s+} + u_{3,\alpha}^{s+})\, dA + \int_{\Omega^+} \tau_{\alpha\beta}^- \delta\varepsilon_{\alpha\beta}^{s-} + \tau_{\alpha 3}^- \delta(u_{\alpha,3}^{s-} + u_{3,\alpha}^{s-})\, dA \\
&= \int_{\Omega^+} \tau_{\alpha\beta}^+ \delta\varepsilon_{\alpha\beta}^{s+} + \tau_{\alpha 3}^+ \delta(u_{3,\alpha}^{s+})\, dA + \int_{\Omega^+} \tau_{\alpha\beta}^- \delta\varepsilon_{\alpha\beta}^{s-} + \tau_{\alpha 3}^- \delta(u_{3,\alpha}^{s-})\, dA.
\end{aligned} \tag{7}$$

By replacing the surface displacements $u_i^{s\pm}$ in (7) with the bulk displacements u_α and w using the displacement continuity conditions in (2), the final surface virtual work becomes

$$\delta U_{\text{surf}} = \int_{\Omega^+} \tau_{\alpha\beta}^+\, \delta\left(u_{\alpha,\beta}^0 - \frac{h}{2} w_{,\alpha\beta}\right) + \tau_{\alpha 3}^+\, \delta(u_{3,\alpha}^{s+})\, dA + \int_{\Omega^+} \tau_{\alpha\beta}^-\left(u_{\alpha,\beta}^0 + \frac{h}{2} w_{,\alpha\beta}\right) + \tau_{\alpha 3}^-\, \delta(u_{3,\alpha}^{s-})\, dA. \tag{8}$$

Here, the domains Ω^+ and Ω^- are defined at $x_3 = +h/2$ and $x_3 = -h/2$, respectively, but are all equal to the midplane domain (Ω) for plate configurations. Therefore, the surface virtual work can be rewritten as

$$\delta U_{\text{surf}} = \int_{\Omega^+} (\tau_{\alpha\beta}^+ + \tau_{\alpha\beta}^-)\, \delta u_{\alpha,\beta}^0 + \frac{h}{2}(-\tau_{\alpha\beta}^+ + \tau_{\alpha\beta}^-)\, \delta w_{,\alpha\beta} + (\tau_{\alpha 3}^+ + \tau_{\alpha 3}^-)\, \delta(w_{,\alpha})\, dA. \tag{9}$$

Then, we can get the final variational equation as follows:

$$\begin{aligned}
\delta\Pi &= \delta U\, (\delta U_{\text{bulk}} + \delta U_{\text{surf}}) - \delta W_E \\
&= \int_\Omega (N_{\alpha\beta} + \tau_{\alpha\beta}^+ + \tau_{\alpha\beta}^-)\, \delta u_{\alpha,\beta}^o - \left\{ M_{\alpha\beta} + \frac{h}{2}(\tau_{\alpha\beta}^+ - \tau_{\alpha\beta}^-) \right\} \delta w_{,\alpha\beta} \\
&\qquad + (\tau_{\alpha 3}^+ + \tau_{\alpha 3}^-)\, \delta w_{,\alpha}\, dA - \int_\Omega p_\alpha\, \delta u_\alpha^0 + p_3\, \delta w\, dA.
\end{aligned} \tag{10}$$

From (10), the following equilibrium equations can be obtained (see the Appendix):

$$N_{\alpha\beta,\beta} + \tau^{+}_{\alpha\beta,\beta} + \tau^{-}_{\alpha\beta,\beta} + p_\alpha = 0, \qquad M_{\alpha\beta,\alpha\beta} + \frac{h}{2}(\tau^{+}_{\alpha\beta,\alpha\beta} - \tau^{-}_{\alpha\beta,\alpha\beta}) + (\tau^{+}_{\alpha 3,\alpha} + \tau^{-}_{\alpha 3,\alpha}) + p_3 = 0. \quad (11)$$

If we set $N^*_{\alpha\beta} = N_{\alpha\beta} + \tau^{+}_{\alpha\beta} + \tau^{-}_{\alpha\beta}$ and $M^*_{\alpha\beta} = M_{\alpha\beta} + \dfrac{h}{2}(\tau^{+}_{\alpha\beta} + \tau^{-}_{\alpha\beta})$, (11) can be simplified as

$$N^*_{\alpha\beta,\beta} + p_\alpha = 0, \quad M^*_{\alpha\beta,\alpha\beta} + (\tau^{+}_{\alpha 3,\alpha} + \tau^{-}_{\alpha 3,\alpha}) + p_3 = 0. \quad (12)$$

The boundary conditions can be of the following forms:

- u^0_α prescribed or $N^*_{\alpha\beta} n_\beta$ specified.
- $\dfrac{\partial w}{\partial n}$ prescribed or $M^*_{\alpha\beta} n_\alpha n_\beta$ specified.
- w prescribed or $\dfrac{\partial (M^*_{\alpha\beta} t_\beta)}{\partial t} + M^*_{\alpha\beta,\beta} + (\tau^{+}_{\alpha 3} + \tau^{-}_{\alpha 3})$ specified.

Constitutive equations for the bulk and surface layers. If the bulk and surface layers are assumed to be homogeneous and isotropic material, the constitutive equation for the bulk layers can be expressed as

$$\sigma_{ij} = \lambda \varepsilon_{kk}\, \delta_{ij} + 2\mu \varepsilon_{ij} + \frac{E\alpha}{1-\nu} \Delta T\, \delta_{ij}, \quad (13)$$

where λ and μ are Lamé's constants, α is the coefficient of thermal expansion, and ΔT is the temperature change. In addition, the face-centered cubic crystal structures exhibit elastic anisotropy, which means the modulus is dependent on orientation. Therefore, the following stress-strain relationship is used for the bulk in this study:

$$\begin{Bmatrix} \sigma_{11} \\ \sigma_{22} \\ \tau_{12} \end{Bmatrix} = \begin{bmatrix} E/(1-\nu^2) & E\nu/(1-\nu^2) & 0 \\ E\nu/(1-\nu^2) & E/(1-\nu^2) & 0 \\ 0 & 0 & G \end{bmatrix} \begin{Bmatrix} \varepsilon_{11} \\ \varepsilon_{22} \\ \gamma_{12} \end{Bmatrix} + \frac{E\alpha}{1-\nu} \begin{Bmatrix} \Delta T \\ \Delta T \\ 0 \end{Bmatrix}, \quad (14)$$

where E and G are the Young's modulus and shear modulus, respectively, and ν is the Poisson's ratio. The constitutive equations for the surface layers are given by [Gurtin and Murdoch 1975a; 1975b; 1978], and these surface constitutive equations are modified to consider the temperature effects by including the surface thermal constant (Θ) [Murdoch 1976]. If the top and bottom surface layers consist of the same material, the equations are expressed as

$$\tau^{\pm}_{\alpha\beta} = \tau_0\, \delta_{\alpha\beta} + (\mu_0 - \tau_0)(u^{\pm}_{\alpha,\beta} + u^{\pm}_{\beta,\alpha}) + (\lambda_0 + \tau_0) u^{\pm}_{\gamma,\gamma}\, \delta_{\alpha\beta} + \tau_0 u^{\pm}_{\alpha,\beta} - \Theta \Delta T^{\pm}\, \delta_{\alpha\beta}, \quad \tau^{\pm}_{\alpha 3} = \tau_0 u^{\pm}_{3,\alpha}, \quad (15)$$

where τ_0 is the surface residual tension, and μ_0 and λ_0 are the surface Lamé's constants.

The surface stress is usually defined as $\tau_{\alpha\beta} = \tau_0\, \delta_{\alpha\beta} + S_{\alpha\beta\gamma\delta} \varepsilon_{\gamma\delta}$ [Miller and Shenoy 2000], where $\tau_{\alpha\beta}$ is the surface stress, $S_{\alpha\beta\gamma\delta}$ is surface elastic modulus tensor, and τ_0 is the surface residual tension when the bulk is unstrained. Therefore, the surface stress $\tau_{\alpha\beta}$ depends on the strain but the constant τ_0 does not change with the relaxation of the thin film with different thicknesses. We obtained this surface residual tension τ_0 from the MD simulations and used it in our finite element model. A rigorous formed surface constitutive relation can be obtained through the surface-Cauchy–Born rule considering atomic potential [Park et al. 2006]. However, the present approach is valid for linearized small deformation problems.

3. Finite element formulation including surface effects

The finite element formulation is derived from the variational equation (10). Before writing the final variational equation for the stiffness matrix, we introduce the necessary notation. First set

$$\boldsymbol{T}_1 = \{\Delta T_1, \Delta T_1, 0\}^T, \qquad \boldsymbol{T}_2 = \{\Delta T_2, \Delta T_2, 0\}^T, \qquad \boldsymbol{T}_m = \{2\tau_0, 2\tau_0, 0\}^T.$$

Then write the generalized resultant forces $\boldsymbol{N}^*$ and moments $\boldsymbol{M}^*$ in matrix form as

$$\begin{Bmatrix} N_{11}^* \\ N_{22}^* \\ N_{12}^* \end{Bmatrix} = \begin{Bmatrix} 2\tau_0 \\ 2\tau_0 \\ 0 \end{Bmatrix} - \left(\frac{Eh\alpha}{1-\nu} + 2\Theta\right)\boldsymbol{T}_1 + \boldsymbol{C}_m \begin{Bmatrix} u_{1,1} \\ u_{2,2} \\ u_{1,2}+u_{2,1} \end{Bmatrix}, \tag{16}$$

$$\begin{Bmatrix} M_{11}^* \\ M_{22}^* \\ M_{12}^* \end{Bmatrix} = -\frac{h^2}{2}\Theta\boldsymbol{T}_2 - \boldsymbol{C}_b \begin{Bmatrix} w_{,11} \\ w_{,22} \\ w_{,12}+w_{,21} \end{Bmatrix}, \tag{17}$$

where the constitutive matrices $\boldsymbol{C}_m$ and $\boldsymbol{C}_b$ for the membrane and bending parts are given by

$$\boldsymbol{C}_m = \begin{bmatrix} \frac{Eh}{1-\nu^2} + 4\mu_0 + 2\lambda_0 & \frac{E\nu h}{1-\nu^2} + 2\lambda_0 + 2\tau_0 & 0 \\ \frac{E\nu h}{1-\nu^2} + 2\lambda_0 + 2\tau_0 & \frac{Eh}{1-\nu^2} + 4\mu_0 + 2\lambda_0 & 0 \\ 0 & 0 & Gh + 2\mu_0 - \tau_0 \end{bmatrix}, \tag{18}$$

$$\boldsymbol{C}_b = \begin{bmatrix} \frac{Eh^3}{12(1-\nu^2)} + \frac{h^2}{2}(2\mu_0+\lambda_0) & \frac{E\nu h^3}{12(1-\nu^2)} + \frac{h^2}{2}(\lambda_0+\tau_0) & 0 \\ \frac{E\nu h^3}{12(1-\nu^2)} + \frac{h^2}{2}(\lambda_0+\tau_0) & \frac{Eh^3}{12(1-\nu^2)} + \frac{h^2}{2}(2\mu_0+\lambda_0) & 0 \\ 0 & 0 & \frac{Gh^3}{12} + \frac{h^2}{2}\mu_0 \end{bmatrix}. \tag{19}$$

We next introduce the vectors

$$\vec{q} = \{u_i, v_i\}^T \quad \text{and} \quad \vec{d} = \{w_i, \theta_{xi}, \theta_{yi}\}^T,$$

representing respectively the nodal degrees of freedom for the membrane components and the element degrees of freedom for the bending components.

Using the area coordinates L_1, L_2, L_3 as interpolation functions, we can write

$$\vec{u} = \sum_{i=1}^{3} \begin{bmatrix} L_i & 0 \\ 0 & L_i \end{bmatrix} \begin{Bmatrix} u_i \\ v_i \end{Bmatrix} = \boldsymbol{N}_m \vec{q} \quad \text{and} \quad w = \sum_{i=1}^{3} \begin{bmatrix} N_i & N_{xi} & N_{yi} \end{bmatrix} \begin{Bmatrix} w_i \\ \theta_{xi} \\ \theta_{yi} \end{Bmatrix} = \boldsymbol{N}_b^T \vec{d} \tag{20}$$

for the interpolation of in-plane displacements $\vec{u}$ (using isoparametric mapping) and the out-of-plane displacement w (using subparametric mapping).

We can now write the final variational equation for the stiffness matrix as

$$\delta\Pi = \delta U - \delta W_E = \int_\Omega \boldsymbol{N}^*\,\delta\vec{\varepsilon} + \boldsymbol{M}^*\,\delta\vec{\psi} + 2\tau_0\,\delta\vec{\phi}\,dA - \int_\Omega \vec{p}\,\delta\vec{u} + \vec{p}_3\,\delta\vec{w}\,dA$$
$$= \int_\Omega \delta\vec{q}^T\boldsymbol{B}_m^T\boldsymbol{T}_m + \delta\vec{q}^T\boldsymbol{B}_m^T\boldsymbol{C}_m\boldsymbol{B}_m\vec{q} - \delta\vec{q}^T\boldsymbol{B}_m^T\Big(\frac{Eh\alpha}{1-\nu} + 2\Theta\Big)\boldsymbol{T}_1 - \delta\vec{d}^T\boldsymbol{B}_b^T\boldsymbol{C}_b\boldsymbol{B}_b\vec{d} + 2\tau_0\,\delta\vec{d}^T\boldsymbol{B}^T$$
$$-\delta\vec{d}^T\boldsymbol{B}_b^T\frac{h^2}{2}\Theta\boldsymbol{T}_2\,dA - \int_\Omega \delta\vec{q}^T\boldsymbol{N}_m^T\vec{p} + \delta\vec{d}^T\boldsymbol{N}_b^T\vec{p}_3\,dA = 0, \quad (21)$$

where

$$\vec{\varepsilon} = \begin{Bmatrix} \partial u/\partial x \\ \partial v/\partial y \\ \partial v/\partial x + \partial u/\partial y \end{Bmatrix} = \sum_{i=1}^{3} \begin{bmatrix} \partial L_i/\partial x & 0 \\ 0 & \partial L_i/\partial y \\ \partial L_i/\partial y & \partial L_i/\partial x \end{bmatrix} \begin{Bmatrix} u_i \\ v_i \end{Bmatrix} \equiv \boldsymbol{B}_m^T\vec{q}, \quad (22)$$

$$\vec{\psi} = \begin{Bmatrix} \partial^2 w/\partial x^2 \\ \partial^2 w/\partial y^2 \\ 2\partial^2 w/\partial x\partial y \end{Bmatrix} = \sum_{i=1}^{3} \begin{bmatrix} \partial^2 N_i/\partial x^2 & \partial^2 N_{xi}/\partial x^2 & \partial^2 N_{yi}/\partial x^2 \\ \partial^2 N_i/\partial y^2 & \partial^2 N_{xi}/\partial y^2 & \partial^2 N_{yi}/\partial y^2 \\ 2\partial^2 N_i/\partial x\partial y & 2\partial^2 N_{xi}/\partial x\partial y & 2\partial^2 N_{yi}/\partial x\partial y \end{bmatrix} \begin{Bmatrix} w_i \\ \theta_{xi} \\ \theta_{yi} \end{Bmatrix} = \boldsymbol{B}_b^T\vec{d}, \quad (23)$$

$$\vec{\phi} = \begin{Bmatrix} \partial w/\partial x \\ \partial w/\partial y \end{Bmatrix} = \sum_{i=1}^{3} \begin{bmatrix} \partial N_i/\partial x & \partial N_{xi}/\partial x & \partial N_{yi}/\partial x \\ \partial N_i/\partial y & \partial N_{xi}/\partial y & \partial N_{yi}/\partial y \end{bmatrix} \begin{Bmatrix} w_i \\ \theta_{xi} \\ \theta_{yi} \end{Bmatrix} = \boldsymbol{B}^T\vec{d}. \quad (24)$$

The vector $\vec{\psi}$ represents the curvature. The load vectors resulting from the temperature change are

$$\int_\Omega \boldsymbol{B}_m^T\Big(\frac{Eh\alpha}{1-\nu} + 2\Theta\Big)\boldsymbol{T}_1\,dA, \qquad \int_\Omega \boldsymbol{B}_b^T\Big(\frac{h^2}{2}\Big)\Theta\boldsymbol{T}_2\,dA,$$

for the membrane and bending components in (21).

In Kirchhoff plate theory, the governing differential equations require transverse displacement and slope continuity across the element boundary, so a nonconforming C^1 continuity finite element is used [Specht 1988; Cho and Parmerter 1994; Oh and Cho 2004; Oh et al. 2008].

In the present study, the thermomechanical surface parameters τ_0, λ_0, μ_0, and Θ are determined by fitting them into the results of MD simulations. The detailed procedure is given in the next section. Once these parameters are determined, the thermomechanical behavior of the nanofilm can be easily analyzed by the present finite element for various thermal and mechanical loading cases.

The geometry and coordinates for the triangular element are shown in Figure 2. For this bending element, the nodal displacement vector $\vec{d}$ is

$$\vec{d}^T = \{w_i, \theta_{xi}, \theta_{yi}\}, \quad (25)$$

where $\theta_{xi} = w_{,y}$ and $\theta_{yi} = -w_{,x}$. The primary unknowns are expressed in terms of nodal variables and shape functions as

$$w = \sum_{i=1}^{3} w_i N_i + \theta_{xi} N_{xi} + \theta_{yi} N_{yi}, \quad (26)$$

where the shape functions N_i, N_{xi}, and N_{yi}, for $i = 1, 2, 3$, can be written as

$$N_i = n_{3i-2}, \qquad N_{xi} = n_{3i-1}, \qquad N_{yi} = n_{3i}.$$

The basis of shape functions in the area coordinate system is given by

$$n_a = \sum_{a=1}^{9} Z_{ar}^{-1} z_r, \qquad a = 1, 2, \ldots, 9, \tag{27}$$

where

$$\begin{aligned}
&z_1 = L_1, && z_2 = L_2, && z_3 = L_3,\\
&z_4 = L_1 L_2, && z_5 = L_2 L_3, && z_6 = L_3 L_1,\\
&z_7 = L_1^2 L_2 + \tfrac{1}{2} L_1 L_2 L_3 \big(3(1-\mu_3) L_1 - (1+3\mu_3) L_2 + (1+3\mu_3) L_3\big),\\
&z_8 = L_2^2 L_3 + \tfrac{1}{2} L_1 L_2 L_3 \big(3(1-\mu_1) L_2 - (1+3\mu_1) L_3 + (1+3\mu_1) L_1\big),\\
&z_9 = L_3^2 L_1 + \tfrac{1}{2} L_1 L_2 L_3 \big(3(1-\mu_2) L_3 - (1+3\mu_2) L_1 + (1+3\mu_2) L_2\big),
\end{aligned} \tag{28}$$

with

$$\mu_1 = \frac{l_3^2 - l_2^2}{l_1^2}, \qquad \mu_2 = \frac{l_1^2 - l_3^2}{l_2^2}, \qquad \mu_3 = \frac{l_2^2 - l_1^2}{l_3^2} \tag{29}$$

(recall from Figure 2 that l_1, l_2, and l_3 are the triangle side lengths), and where the inverse transformation matrix is given by

$$Z_{ar}^{-1} = \begin{bmatrix}
1 & 0 & 0 & -1 & 0 & 1 & 2 & 0 & -2\\
0 & 0 & 0 & 0 & 0 & a_{12} & -a_{13} & 0 & -a_{12}\\
0 & 0 & 0 & 0 & 0 & a_{22} & -a_{23} & 0 & -a_{22}\\
0 & 1 & 0 & 1 & -1 & 0 & -2 & 2 & 0\\
0 & 0 & 0 & a_{13} & 0 & 0 & -a_{13} & -a_{11} & 0\\
0 & 0 & 0 & a_{23} & 0 & 0 & -a_{23} & -a_{21} & 0\\
0 & 0 & 1 & 0 & 1 & -1 & 0 & -2 & 2\\
0 & 0 & 0 & 0 & a_{11} & 0 & 0 & -a_{11} & -a_{12}\\
0 & 0 & 0 & 0 & a_{21} & 0 & 0 & -a_{21} & -a_{22}
\end{bmatrix}, \tag{30}$$

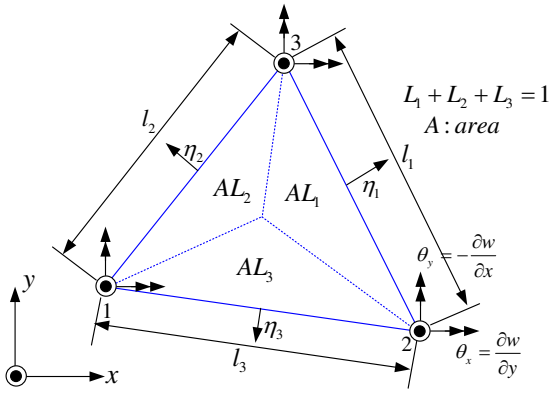

Figure 2. Geometry and coordinates for plate bending element with nine degrees of freedom.

with

$$[a_{ij}] = \left[2A\frac{\partial L_j}{\partial x_i}\right] = \begin{bmatrix} y_2 - y_3 & y_3 - y_1 & y_1 - y_2 \\ x_3 - x_2 & x_1 - x_3 & x_2 - x_1 \end{bmatrix}.$$

The determination of z_7, z_8, and z_9 is based on the following considerations. From the boundary conditions, the energy associated with interelement jumps can be written

$$\Delta U_{\Gamma_s} = \int_{\Gamma_s} M^*_{nn}\,\Delta\left(\frac{\partial w}{\partial n}\right) d\Gamma + \int_{\Gamma_s} M^*_{ns}\,\Delta\left(\frac{\partial w}{\partial s}\right) d\Gamma. \tag{31}$$

Physically, there should be no energy associated with these interelement discontinuities; so we set both terms of (31) to zero.

Since $w(s)$ is uniquely determined from the two node data, $\Delta w_{,s}$ is equal to zero. For a constant state of bending moments, the following condition should be required to pass the bending patch test:

$$M^*_{nn}\int_{\Gamma_s} \Delta\left(\frac{\partial w}{\partial n}\right) d\Gamma = 0. \tag{32}$$

Thus the quadric polynomials z_7, z_8, and z_9 are determined to satisfy (32). The transformation matrix Z_{ar} is regular for an arbitrary geometry of the triangle.

As is seen above, each of the constitutive matrices for the membrane and bending components contains the surface parameters which represent the surface effects. The membrane and bending stiffness matrices, which are required for the finite element implementation, can be expressed as follows from (21):

$$\boldsymbol{K}_m = \int_\Omega \boldsymbol{B}_m^T \boldsymbol{C}_m \boldsymbol{B}_m\, dA, \qquad \boldsymbol{K}_b = \int_\Omega \boldsymbol{B}_b^T \boldsymbol{C}_b \boldsymbol{B}_b\, dA. \tag{33}$$

4. Molecular dynamics simulations

Determination of surface parameters. The accuracy of the solution obtained from the finite element analysis based on the continuum model, which considers surface effects, is dependent on the reliability of the surface parameters τ_0, μ_0, and λ_0.

Generally, these parameter values can be provided by experiments or MD simulations. In this study, the necessary surface parameters are obtained from MD simulations with open source code [LAMMPS 2008].

Figure 3 shows the configuration of the unit cell of copper thin film. The periodic boundary conditions are applied along the x_1 and x_2 directions, and the free boundary condition is applied in the x_3 direction. The dimensions of the unit cell are about 20 nm for the x_1 and x_2 directions, and 4.3 nm in the x_3

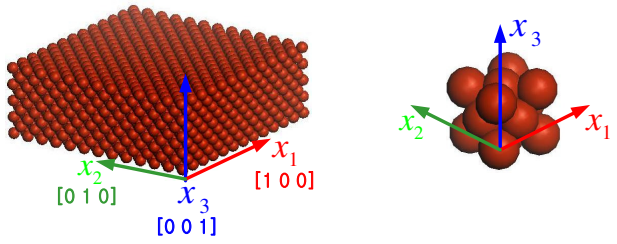

Figure 3. Molecular dynamics simulation model for copper thin film with (100) surface.

direction. The simulation temperature is 0.1 K. The surface crystallographic orientation of the unit cell is the (100). The simulation cell size to get the bulk properties of copper is about 20 nm in all directions and the simulation cell satisfies the periodic boundary conditions in the x_1 [100], x_2 [010] and x_3 [010] directions respectively. The surface parameter values (τ_0, μ_0, and λ_0) are provided by MD simulations with the embedded atom method potential for the copper thin film. To determine the surface stress, energy minimization is performed for the atoms at the surface to obtain their equilibrium positions. The simulation cell, shown in Figure 3, is then strained to calculate the total energy. The total energy of the thin film consists of the strain energy in the bulk and on the surface; therefore, the surface energy must be extracted from the total energy. If the area of the surface is defined as $A\ (= dx_1 dx_2)$, the total energy can be expressed as a function of strain [Shenoy 2005]: $E_{\text{total}} = E_{\text{surface}} + E_{\text{bulk}} = 2AE_s(\varepsilon) + hAE_b(\varepsilon)$, where $E_s(\varepsilon)$ and $E_b(\varepsilon)$ are the surface energy and bulk energy, respectively. The total energy is linear with respect to the thickness h of the thin film. Therefore, the linear fit, which is made with the E_{total} and h data, can give the surface energy. Once the total surface energy is obtained, the surface stress can be obtained from the definition of surface stress: $\tau_{ij}^0 = 1/A(\partial E_{\text{surface}}/\partial \varepsilon_{ij})_{\varepsilon=0}$ [Haiss 2001]. The obtained surface residual tension for copper with a (100) surface is $\tau_0 = 1.0398$ N/m.

The MD simulation is performed as well and two elastic constants (C_{11} and C_{12}) can be obtained. A thin film with (100) surface orientation has the same directional properties in the x_1 [100] and x_2 [010] directions. Therefore, it is possible to calculate both C_{11} and C_{22} just with one simulation because the thin film structure has the same C_{11} and C_{22} components in this orientation. But, the thin film with (110) surface orientation has different directional properties along the [100] and [110] directions. So, the values of C_{11} and C_{22} are different from each other. Two times the strain tests with respect to ε_{11} and ε_{22} are required to calculate C_{11}, C_{22}, and C_{12} respectively. The simulation cell is strained along the x_1 direction, that is, ε_{11} has a specific value while constraining the deformation along the x_2 direction ($\varepsilon_{22} = 0$). The correlation between components of the constitutive matrix for the membrane part of the finite element model (see (18)) and the corresponding two elastic constants from the MD simulations yield the equations

$$C_{11} = \frac{Eh}{1-\nu^2} + 4\mu_0 + 2\lambda_0, \qquad C_{12} = \frac{E\nu h}{1-\nu^2} + 2\lambda_0 + 2\tau_0. \tag{34}$$

Here all variables except μ_0 and λ_0 are already known, so the two unknown surface constants are easily determined to be $\mu_0 = -8.755$ N/m and $\lambda_0 = 15.843$ N/m at the matching point. The surface parameter values do not vary significantly as shown in Table 1 for the films with different thicknesses. Here, the surface residual tension is assumed to be constant as mentioned above.

thickness (Å)	τ_0	μ_0	λ_0
14.72	1.0398	−8.571	15.432
29.25	1.0398	−8.643	15.638
43.75	1.0398	−8.755	15.843

Table 1. Surface parameter values.

After the three surface constants are determined, the surface thermal constant is also obtained from the results of the MD simulations. The temperature is increased from 0 K to 500 K, and the thermal strains are calculated at every 100 K increment during the simulations.

A certain amount of deviation in the results cannot be avoided due to the nature of MD simulations; this deviation tends to be larger as the temperature increases. This is the reason why MD simulations are usually performed several times and averaged values taken. Here, the average of thermal strain can be considered to be uniform in a relatively low temperature range as shown in the graph (the black solid line in Figure 4a). Consequently, the averaged strain values are obtained as $u_{1,1} = 0.001291$ and $u_{2,2} = 0.001268$ (see Table 2). From the constitutive relation about the membrane components described in (16), we obtain the following relation:

$$N_{11}^* = 2\tau_0 - \left(\frac{Eh\alpha}{1-\nu} + 2\Theta\right)\Delta T_1 + \left(\frac{Eh}{1-\nu^2} + 4\mu_0 + 2\lambda_0\right)u_{1,1} + \left(\frac{E\nu h}{1-\nu^2} + 2\lambda_0 + 2\tau_0\right)u_{2,2}. \tag{35}$$

Here, because N_{11}^* is zero due to the stress free condition and all other variables are known except the surface thermal constant (Θ), the surface thermal constant is determined to be $\Theta = -3.216 \times 10^{-4}$. A more detailed procedure for finding the equilibrium state and straining process can be found in the next section.

We could also observe an almost constant coefficient of thermal expansion (CTE) of the copper thin film in the temperature range lower than 500 K from the MD simulations in Figure 4b. It is thus reasonable to use the proposed model in the smaller temperature range assuming small temperature variance.

Modulus computations of copper thin film with thickness variations. The mechanical properties of thin films with different thicknesses, such as the Young's modulus, the shear modulus, and the Poisson's ratio, are provided by the MD simulations and compared with the FEM results. In this study, we consider two configurations: (100) surface orientation and [100] loading direction ((100)/[100]) and (100) surface orientation and [110] loading direction ((100)/[110]). Figure 6 shows the simulation configurations and coordinate systems. The simulation conditions are basically the same as those explained in the previous section except for thickness variations.

We have five simulation models for the thin film with different thicknesses:

$$h = 14.64, 29.11, 43.62, 58.23, 115.98\,(\text{Å}).$$

The first step of MD simulation is to find the equilibrium states of the simulation cells. To this end, the NPT ensemble (the number of atoms, pressure, and temperature of the system will remain

Temp. (K)	$\varepsilon_{11}(u_{1,1})$	$\varepsilon_{22}(u_{2,2})$
100	0.001252	0.001281
200	0.001257	0.001234
300	0.001402	0.001228
400	0.001079	0.001421
500	0.001466	0.001178
Avg.	0.001291	0.001268

Table 2. Strains caused by temperature change.

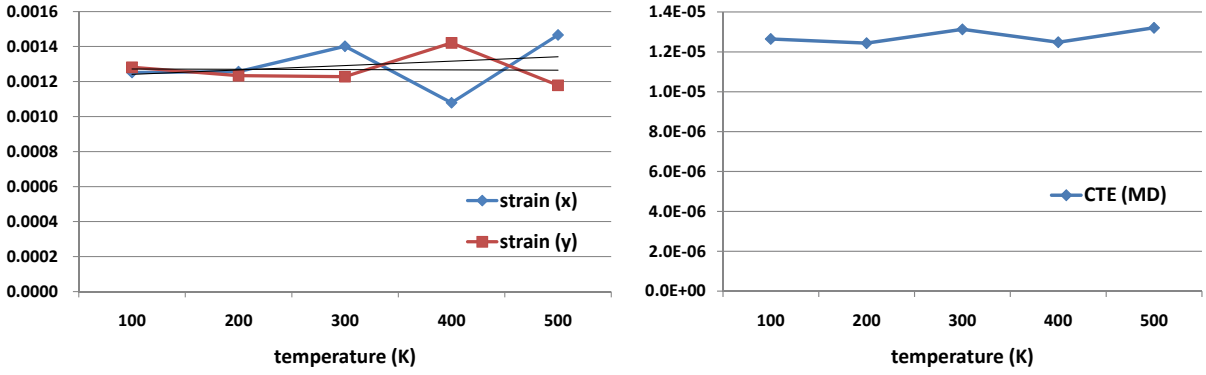

Figure 4. Strain variance (a) and CTE variance (b) where the simulation cell thickness is 3.62 nm (matching point).

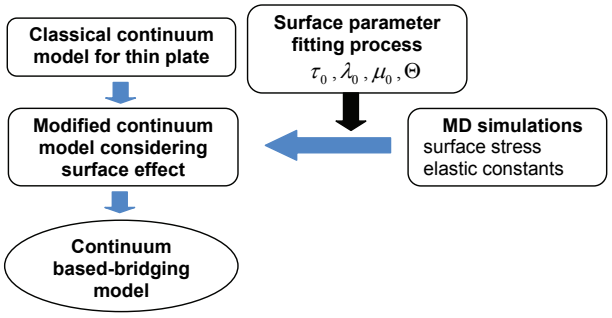

Figure 5. Overall process of continuum based-bridging model development.

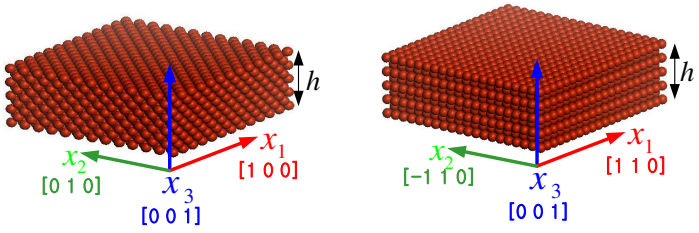

Figure 6. MD simulation model for the copper thin film: under (100)/[100] configuration (left) and (100)/[110] configuration (right).

constant) is adopted and we set the initial conditions of temperature, pressure, and lattice constant (a_0) as $T = 0.1$ K, $P = 0$ bar, and $a_0 = 0.362$ nm, respectively. As mentioned in the previous section, the simulation cell boundary lateral surfaces satisfy periodic boundary conditions and the bounding surface in the x_3 direction is free. MD simulation up to 100 ps is performed with the NPT ensemble to get the equilibrium state, followed by the NVT ensemble (where the number of atoms, volume, and temperature of the system will remain constant) for 50 ps to obtain the initial stresses. Then the simulation cell is strained as $\varepsilon = 0.01$ for 100 ps in each step and the averaged stress is calculated under the equilibrium

state. Finally, the mechanical properties of the thin film are computed based on the obtained stress and strain relation. The simulation results are given in the following chapter for both thin film configurations.

5. Numerical examples

Mechanical properties: Young's modulus, shear modulus, and Poisson's ratio. The elastic properties of thin film can be different with respect to the surface orientation and loading direction. In this study, the elastic properties are obtained from FEM simulation and compared with MD simulation results under two configurations as mentioned in the previous chapter.

A tensile test for the Cu thin film is performed to compute the Young's modulus and Poisson's ratio with the proposed FEM based on continuum theory considering surface effects. The pure shear test is also carried out to compute the shear modulus. As explained in the previous section, the surface parameter values are obtained from the MD simulations when the thickness of the copper thin film is about 43 Å, that is, this is the matching point between the finite element model and the MD simulations. If the necessary surface parameters are determined at this point, we do not need to do any more MD simulations about the thin film with other thickness dimensions to determine surface parameters. This means that the suggested continuum model does not require excessive computing time and can give us the mechanical response of the thin film in a very short period of time. The rest of the moduli of the thin film with different thicknesses can be calculated by the continuum based-finite element model with the fitted surface parameter values.

In each simulation, 200 finite elements are used as depicted in Figure 7, which also represents the deformed configuration of the thin film model due to surface effects only. When there are no externally applied forces, the thin film with positive surface stress shrinks to be in a relaxed state. As is shown in the left part of Figure 8, the modulus of the thin film with (100) surface and [100] loading direction is smaller than that of the bulk material by 23% when the thickness is about 14 Å. However, the modulus

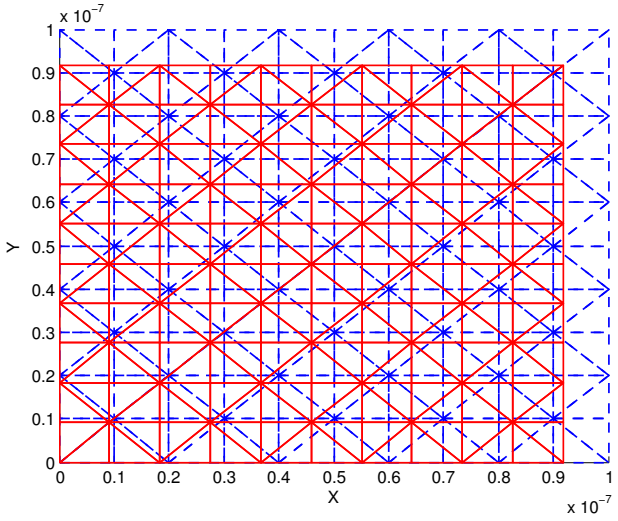

Figure 7. Initial finite element mesh configuration (blue dashed line) and relaxation due to surface effects only (red solid line).

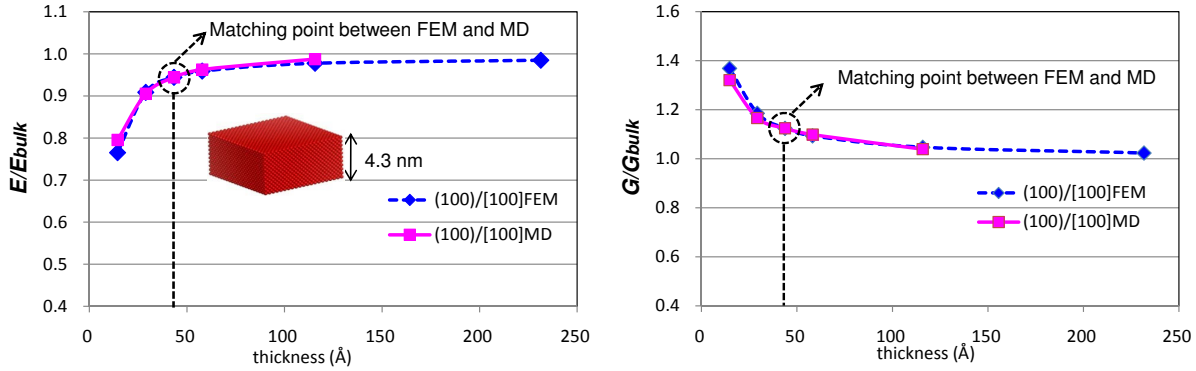

Figure 8. Young's modulus (left) and shear modulus (right) of a copper thin film with (100) surface, and under [100] loading.

converges to the bulk counterpart as the thickness increases. The moduli calculated by the FEM agree well with the results from the MD simulation. This softening phenomenon can be explained by the atomic coordination. The atomic coordination is low on the surfaces compared to the bulk and the modulus tends to be softer. From MD simulations, the elastic constant of a surface with the (100)/[100] configuration is negative due to the bond loss. Considering that total stiffness is equal to bulk stiffness plus surface stiffness, negative surface stiffness causes the overall stiffness of thin film to be smaller than the bulk counterpart. Moreover, this effect becomes more dominant as the thickness gets smaller as shown in Figure 8, left. Similar phenomena have also been observed by other researchers [Miller and Shenoy 2000; Gao et al. 2006]. The bulk Young's modulus (E) of a single crystal structured copper, which is used in this study, is about 62.09 GPa and the bulk shear modulus (G) is 76.46 GPa. The Poisson's ratio (ν) is 0.424. These values are obtained by MD simulation for the bulk copper material and are very close to the reference values [Simmons and Wang 1971].

Figure 8, right, compares the shear moduli predicted by the FEM and MD calculations. Unlike the Young's modulus, the shear modulus is larger for thin films that its bulk value, and it converges to its bulk counterpart as the thickness increases. To our knowledge, the literature does not so far contain predictions of shear modulus for a thin film. The shear modulus is calculated by the relation $\tau = G\gamma$ where τ, G, and γ are the virial stress, shear modulus, and engineering shear strain. The MD simulation is carried out in the shear strained unit cell configuration. Virial stress is obtained as a result of the MD simulation, and increases as the thickness gets smaller, because the pairwise interaction forces between atoms increase due to the contraction effect caused by surface stress.

The results of the Poisson's ratio of a copper thin film with (100) surface are plotted in Figure 9. For a thin film under [100] loading direction, the Poisson's ratio becomes larger than the bulk counterpart when the thickness gets smaller. The Poisson's ratio is defined as $\nu = -\varepsilon_{yy}/\varepsilon_{xx}$, where ε_{xx} and ε_{yy} are the strains along the x and y directions. In the case of a thin film with the (100)/[100] configuration, greater contraction in the y direction and less extension in the x direction are observed due to positive surface stress, because a thin film with positive surface stress shrinks in a relaxed state. Therefore, when the thickness of the thin film is smaller, a larger Poisson's ratio is observed. The results of the FEM agree with those of the MD simulations.

	MD			FEM		
h (Å)	C_{11}, C_{22}	C_{12}	C_{66}	C_{11}, C_{22}	C_{12}	C_{66}
14.64	99.59	70.70	100.98	100.68	73.16	106.77
29.11	87.63	52.48	89.18	87.99	52.72	91.18
43.62	83.73	45.86	85.95	83.73	45.86	85.95
58.23	81.11	41.60	84.01	81.60	42.42	83.33
115.98	77.52	35.44	79.46	78.38	37.24	79.38

Table 3. Elastic constants of single crystal copper thin film with (100) surface orientation and [100] loading direction.

In this study, we consider a face centered cubic (FCC) material which has cubic symmetry. The elastic deformation of this material can be represented by the three constants C_{11}, C_{12}, and C_{66} in the Voigt notation. These elastic constants of a single crystal copper thin film with (100) surface orientation and [100] loading direction are computed by MD simulations and FEM according to the change in the thickness and are tabulated in Table 3. The corresponding elastic constants from the MD simulation and FEM are almost the same.

For a thin film under the (100)/[110] configuration, the stiffness of the thin film can be regarded as a 45° rotation of the (100)/[100] thin film configuration, as depicted in Figure 10. So it is expected that the elastic constants from MD simulations about the (100)/[110] configuration would be the same as those computed by using the elastic constants of the (100)/[100] thin film configuration through the stiffness transformation relationship between the two configurations [Tsai and Hahn 1980].

The MD simulation for copper thin film with the (100)/[110] configuration is performed and elastic constants are obtained (MD (I)). These are compared with the transformed elastic constants (MD (II)) of the thin film with the (100)/[100] configuration in Table 4. The corresponding quantities are similar

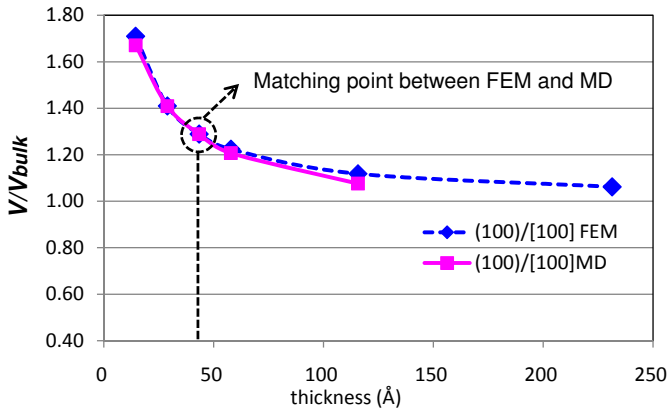

Figure 9. Poisson's ratio of a copper thin film with (100) surface and under [100] loading direction, where a dotted circle indicates the matching point between the result of the FEM and that of the MD simulations.

	MD (I)			MD (II)			FEM		
h (Å)	C_{11}, C_{22}	C_{12}	C_{66}	C_{11}, C_{22}	C_{12}	C_{66}	$C_{11}C_{22}$	C_{12}	C_{66}
14.64	179.11	−17.70	14.65	186.12	−15.83	14.44	193.69	−19.84	13.76
29.11	153.39	−20.19	17.91	159.24	−19.12	17.57	161.54	−20.83	17.64
43.62	145.46	−20.87	18.57	150.74	−21.15	18.94	150.74	−21.15	18.94
58.23	143.35	−21.20	19.12	145.36	−22.65	19.75	145.34	−21.32	19.59
115.98	134.57	−22.10	20.61	135.93	−22.98	21.04	137.19	−21.57	20.57

Table 4. Elastic constants of single crystal copper thin film with (100) surface orientation and [110] loading direction.

to each other and the elastic constants obtained by FEM are also close to both the MD (I) and MD (II) simulation results in the thin film with different thicknesses.

The comparison of the Young's modulus and shear modulus of thin film with (100) surface orientation and [110] loading direction between the MD simulations and FEM is shown in Figure 11. But the trend of variations of the Young's modulus and shear modulus is opposite to those of the thin film with the (100)/[100] configuration. Especially for the Young's modulus, the modulus gets larger than bulk counterpart as the thickness becomes smaller. FEM results also show good agreement with those of the MD simulations.

From the results shown above, there is an obvious size effect for mechanical properties of nanosized thin film with thickness variations. In addition, the mechanical properties for a single crystal structure are strongly dependent on the loading directions.

Bending rigidity and the coefficient of thermal expansion. The surface effects are also introduced in bending as an additional force. The flexural rigidity of the bulk thin plate is $D_b = \frac{1}{12}Eh^3/(1-\nu^2)$ and the flexural rigidity of thin film is $D_f = \frac{1}{12}Eh^3/(1-\nu^2) + \frac{1}{2}h^2(2\mu_0 + \lambda_0)$, while the nondimensional flexural rigidity is plotted in Figure 12. The quantity $(D_f - D_b)/D_b$ for the thin film with the (100)/[100] configuration becomes small with decreasing thickness because negative surface stiffness also softens the flexural rigidity. But it tends to converge in the opposite way in the case of the thin film with the (100)/[110] configuration. Figure 13 shows the comparison of the CTE from the FEM and MD simulations. The bulk value of the CTE is obtained as 1.65×10^{-5}/K from the MD simulations, which is

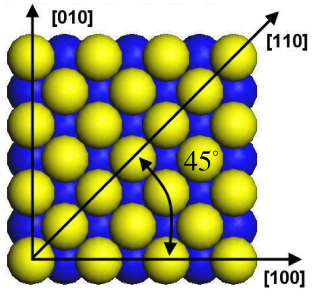

Figure 10. Top view of the (100) surface of FCC copper thin film.

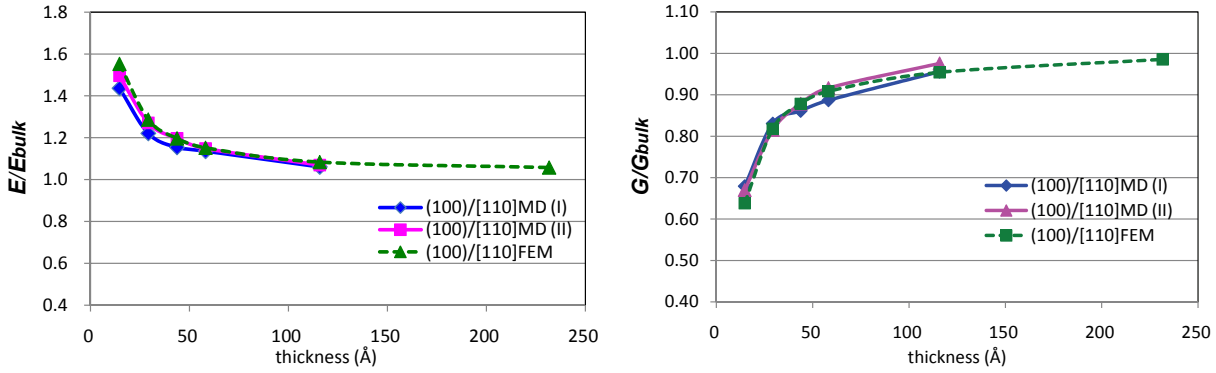

Figure 11. Young's modulus of a copper thin film (left) and shear modulus with (100) surface and under [110] loading direction (right).

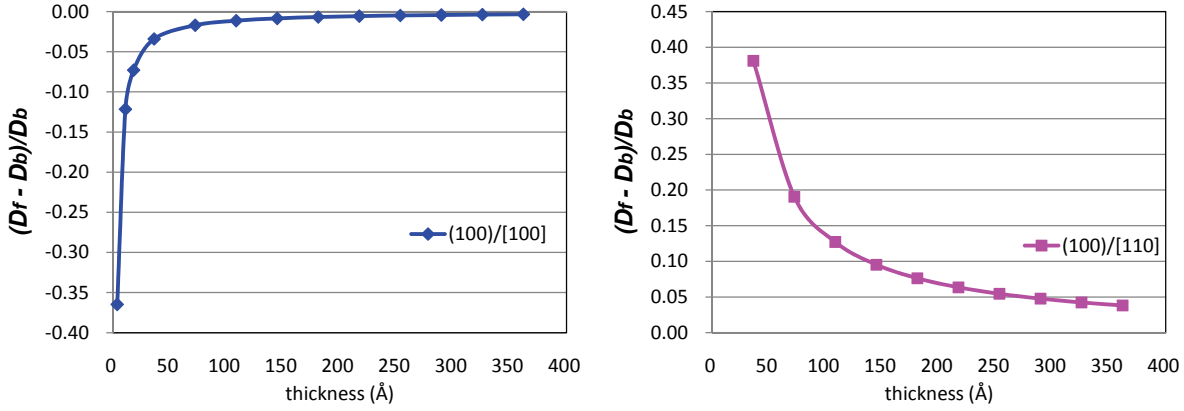

Figure 12. Nondimensional flexural rigidity: copper thin film with (100)/[100] configuration (left) and copper thin film with (100)/[110] configuration (right).

almost the same as the reference value [Shackelford and Alexander 2000]. The CTE of a copper thin film with (100) surface decreases as the thickness of the film decreases [Pathak and Shenoy 2005]. Generally, the change in the film area with temperature can be written as $\Delta A/A_0 = \alpha \Delta T$, where ΔA is the change of area, A_0 is the initial area, and α is the CTE. Temperature rise usually expands the size of the thin film. But when the thickness gets smaller, the role of surface stress becomes more prominent and the positive surface stress tends to shrink the thin film. Therefore, the area of the film is decreased and the CTE of the thin film becomes smaller than that of the bulk. For a thin film with FCC (100) surface orientation, it exhibits in-plane symmetry so that the CTE does not change with respect to the directions.

Buckling analysis. To investigate how the surface effect affects the buckling behavior of the nano thin film, the buckling analysis is carried out for free standing copper thin film.

For a thin film, the strain energy subjected to in-plane forces can be written as $U = U_b + U_s$, where U_b is the strain energy due to the bending including surface effects and U_s is the strain energy due to the

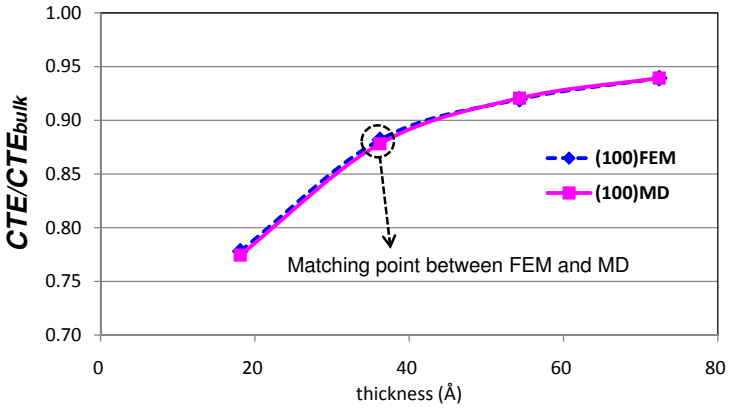

Figure 13. CTE of a copper thin film with a (100) surface. ($\mathrm{CTE}_{\mathrm{bulk}}(\alpha_{\mathrm{bulk}}) = 1.65 \times 10^{-5}$ /K).

in-plane forces, given by [Abbas and Thomas 1977]

$$U_s = \frac{1}{2}\int_\Omega \left[N_{11}\left(\frac{\partial w}{\partial x_1}\right)^2 + N_{22}\left(\frac{\partial w}{\partial x_2}\right)^2 + 2N_{12}\left(\frac{\partial w}{\partial x_1}\right)\left(\frac{\partial w}{\partial x_2}\right)\right] dA, \qquad N_{\alpha\beta} = \int_{-h/2}^{h/2} \sigma_{\alpha\beta}\, dz, \tag{36}$$

or, in matrix form,

$$U_s = \frac{1}{2}\int_\Omega \begin{bmatrix} \dfrac{\partial w}{\partial x_1} & \dfrac{\partial w}{\partial x_2} \end{bmatrix} \begin{bmatrix} N_{11} & N_{12} \\ N_{12} & N_{22} \end{bmatrix} \begin{bmatrix} \dfrac{\partial w}{\partial x_1} \\ \dfrac{\partial w}{\partial x_2} \end{bmatrix} dA. \tag{37}$$

By using the derivative of the lateral displacement w given in (20), we have

$$U_s = \frac{1}{2}\int_\Omega \{\vec{d}\}^T \boldsymbol{B}^T [\boldsymbol{N}] \boldsymbol{B} \{\vec{d}\}\, dA. \tag{38}$$

The differentiation in (38) with respect to the nodal displacements gives a geometric stiffness:

$$[\boldsymbol{K}_s] = \int_\Omega \boldsymbol{B}^T [\boldsymbol{N}] \boldsymbol{B}\, dA. \tag{39}$$

We assemble the element matrices to get the static stability matrix equation

$$([\boldsymbol{K}_b] - \lambda[\boldsymbol{K}_s])\{\vec{d}\} = 0, \tag{40}$$

where λ is the buckling load. Equation (40) was solved for a thin film structure with simply supported boundary conditions, and the results are shown in Figure 14. For copper thin film with a (100) surface orientation, the buckling parameter $K = N^* b^2/(\pi^2 D)$ of the film becomes smaller as the thickness decreases, due to surface effects. The surface effects do not change the fundamental buckling mode shape, shown in Figure 15. As the thickness increases, the buckling parameter value converges to the bulk value obtained by ignoring surface effects.

The buckling of a thin film with high aspect ratio ($a/b = 10$) was considered next, and the results are shown in Figure 16. All edges are clamped in the left half of the figure and simply supported the right half. Again, there is no change in fundamental buckling mode shape due to the surface effects, but the

buckling parameter values of the thin film considering surface effects are lower than those of the bulk when the thickness becomes smaller, as shown in Figures 14 and 16.

The postbuckling behavior of the nano thin film is quite different from that of the proposed continuum plate behavior with the size effect. The atomistic potential behavior is totally different from the continuum linear elastic behavior because the atomic behavior includes the highly geometric nonlinear effect as well as the inelastic effects such as twining and slip. However, the onset of instability can be reasonably well described by the linear elastic buckling analysis. Thus the linear buckling analysis of nanoscale thin films can provide a guideline for the onset of structural instability.

6. Conclusions

In this study, a continuum model considering of the surface effects of thin film is suggested and a finite element formulation is also implemented. Because this continuum model is properly modified for nano sized thin film by adding the surface energy contribution to the classical thin plate theory in the

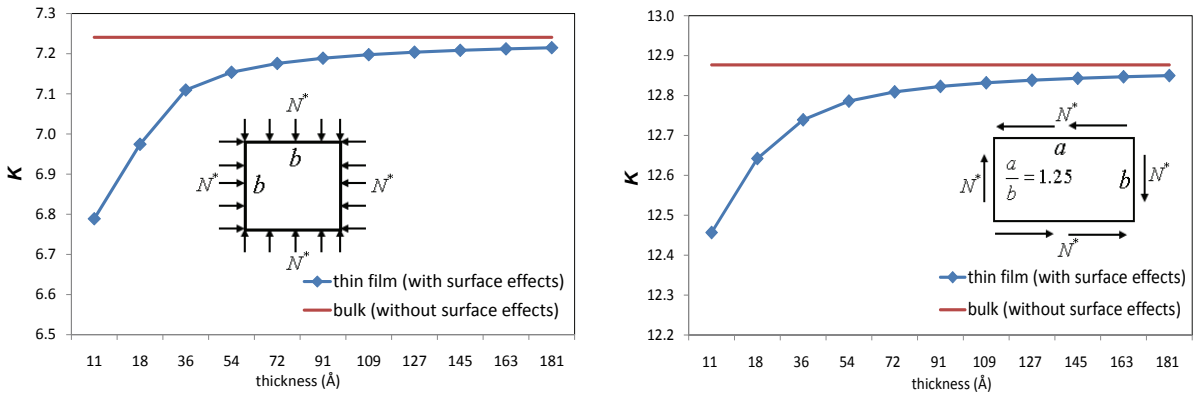

Figure 14. Buckling parameter K for a roughly square copper thin film with a (100) surface is clamped on all edges and compressed biaxially (left), or simply supported on all edges and subjected to pure shear (right).

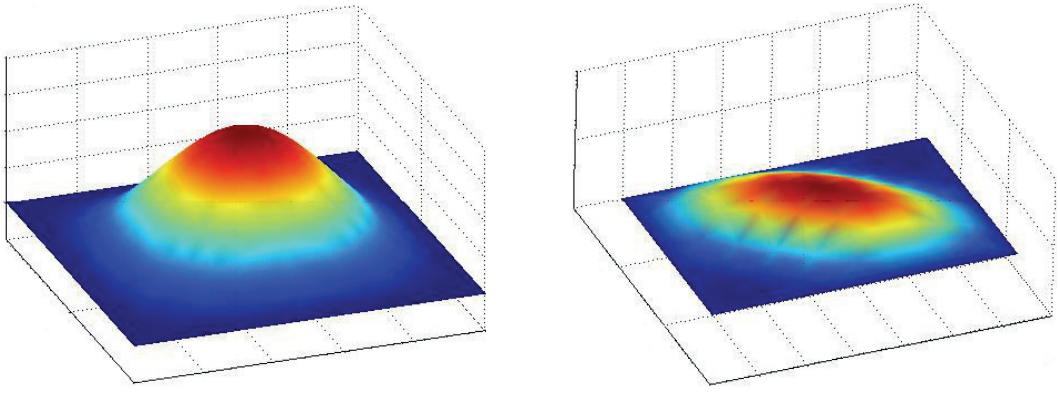

Figure 15. Shape of fundamental buckling mode for the experiments of Figure 14.

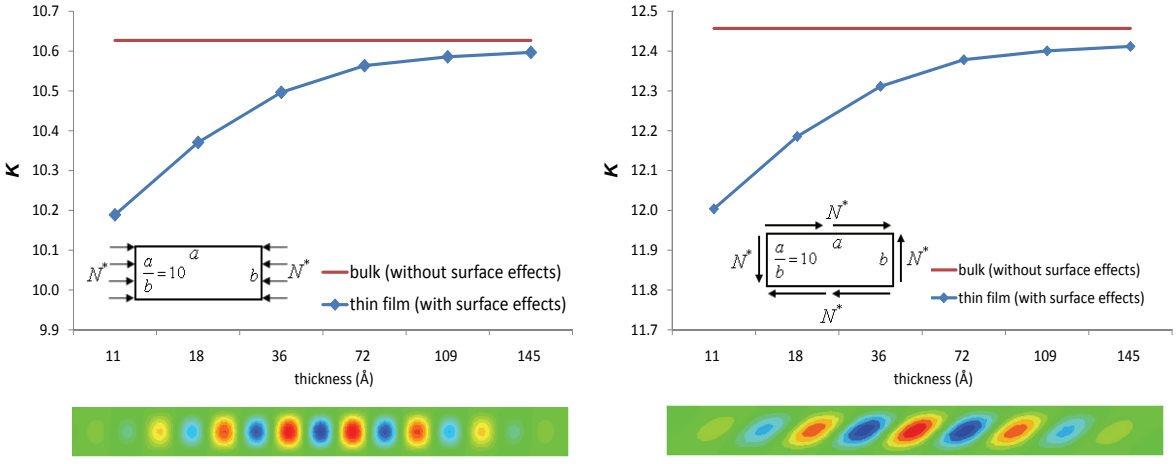

Figure 16. A strip of copper thin film with a (100) surface is clamped on all edges and compressed uniaxially (left), or alternatively simply supported on all edges and subjected to pure shear (right). Top: buckling parameters; bottom: shape of fundamental buckling mode.

macroscale, it can represent the dominant surface effects which should be considered in nanoscale thin film structures.

The suggested continuum model should serve as a useful alternative method to overcome the limitations of conventional molecular dynamics (MD) simulations, such as excessive required computing resources and time. The proposed continuum model can also be used when we need to carry out the design modification and analysis process repeatedly for practical applications in the mesoscale range. To accurately predict the properties of thin film structures, reliable material constants of its bulk and surface should be known. Therefore, precise measurement techniques and MD simulation methods are essential factors. The thermomechanical responses of the thin film with other surface orientations will be addressed in future.

Appendix: Equilibrium equations and boundary conditions

The principle of virtual work states that the stress, body force, and traction are in equilibrium if and only if the internal virtual work equals the external virtual work for every virtual displacement field. Therefore, the following equation can be derived by applying integration by parts and the divergence theorem to obtain the equilibrium equations from (10):

$$\delta\Pi = \int_{\Omega} -(N_{\alpha\beta,\beta} + \tau^{+}_{\alpha\beta,\beta} + \tau^{-}_{\alpha\beta,\beta})\,\delta u^{o}_{\alpha} - \left\{M_{\alpha\beta,\alpha\beta} + \frac{h}{2}(\tau^{+}_{\alpha\beta,\alpha\beta} - \tau^{-}_{\alpha\beta,\alpha\beta})\right\}\delta w \\ - (\tau^{+}_{\alpha 3,\alpha} + \tau^{-}_{\alpha 3,\alpha})\,\delta w - p_{\alpha}\,\delta u^{o}_{\alpha} - p_{3}\,\delta w\,dA + \text{Boundary Conditions}. \quad \text{(A.1)}$$

The boundary terms are summarized as the following. First, the boundary conditions of the bulk part are considered:

$$\delta U^{\text{boundary}}_{\text{bulk}} = \int_{\partial S} N_{\alpha\beta} n_{\beta}\,\delta u^{0}_{\alpha} + M_{\alpha\beta,\beta} n_{\beta}\,\delta w - M_{\alpha\beta} n_{\beta}\,\delta w_{,\alpha}\,dS. \quad \text{(A.2)}$$

The boundary conditions are usually expressed in terms of directions that are normal and tangent to the boundaries. Therefore, the derivatives of w in Cartesian coordinates can be represented in terms of derivatives in the normal direction ($\partial w/\partial n$) and the tangent direction ($\partial w/\partial t$) of the boundary:

$$w_{,\alpha} = \frac{\partial w}{\partial n} n_\alpha + \frac{\partial w}{\partial t} t_\alpha. \tag{A.3}$$

Substituting (A.3) into (A.2) we obtain

$$\begin{aligned}
\delta U_{\text{bulk}}^{\text{boundary}} &= \int_{\partial S} N_{\alpha\beta} n_\beta \, \delta u_\alpha^0 + M_{\alpha\beta,\beta} n_\beta \, \delta w - M_{\alpha\beta} n_\beta \, \delta w_{,\alpha} \, dS \\
&= \int_{\partial S} N_{\alpha\beta} n_\beta \, \delta u_\alpha^0 + M_{\alpha\beta,\beta} n_\beta \, \delta w - M_{\alpha\beta} n_\beta \, \delta\Big(\frac{\partial w}{\partial n} n_\alpha + \frac{\partial w}{\partial t} t_\alpha\Big) \, dS \\
&= \int_{\partial S} N_{\alpha\beta} n_\beta \, \delta u_\alpha^0 + M_{\alpha\beta,\beta} n_\beta \, \delta w - M_{\alpha\beta} n_\beta n_\alpha \, \delta\Big(\frac{\partial w}{\partial n}\Big) - M_{\alpha\beta} n_\beta t_\alpha \Big(\frac{\partial w}{\partial t}\Big) \, dS,
\end{aligned} \tag{A.4}$$

where the fourth term can be changed to the following form through integration by parts:

$$\int_{\partial S} M_{\alpha\beta} n_\beta t_\alpha \Big(\frac{\partial w}{\partial t}\Big) \, dS = \Big[M_{\alpha\beta} n_\beta t_\alpha \Big(\frac{\partial w}{\partial t}\Big) \Big]_{S_1}^{S_2} - \int_{\partial S} \Big(\frac{\partial M_{\alpha\beta} n_\beta t_\alpha}{\partial t} \Big) \delta w \, dS. \tag{A.5}$$

If the boundary is a closed smooth curve, the start and end points are the same and the first term vanishes in above equation. Therefore, the final form of the boundary condition for the bulk part is given as

$$\delta U_{\text{bulk}}^{\text{boundary}} = \int_{\partial S} N_{\alpha\beta} n_\beta \, \delta u_\alpha^0 - M_{\alpha\beta} n_\beta n_\alpha \, \delta\Big(\frac{\partial w}{\partial n}\Big) + \Big(\frac{\partial (M_{\alpha\beta} n_\beta t_\alpha)}{\partial t} + M_{\alpha\beta,\beta} n_\beta \Big) \delta w \, dS. \tag{A.6}$$

Next, the boundary conditions about surface layers are considered:

$$\begin{aligned}
\delta U_{\text{surface}}^{\text{boundary}} &= \int_{\partial S} (\tau_{\alpha\beta}^+ - \tau_{\alpha\beta}^-) n_\beta \, \delta u_\alpha^0 - \frac{h}{2} (\tau_{\alpha\beta}^+ - \tau_{\alpha\beta}^-) n_\beta \, \delta w_{,\alpha} \\
&\qquad + \frac{h}{2} (\tau_{\alpha\beta,\beta}^+ - \tau_{\alpha\beta,\beta}^-) n_\alpha \, \delta w + (\tau_{\alpha 3}^+ + \tau_{\alpha 3}^-) n_\alpha \, \delta w \, dS \\
&= \int_{\partial S} (\tau_{\alpha\beta}^+ - \tau_{\alpha\beta}^-) n_\beta \, \delta u_\alpha^0 - \frac{h}{2} (\tau_{\alpha\beta}^+ - \tau_{\alpha\beta}^-) n_\alpha n_\beta \, \delta\Big(\frac{\partial w}{\partial n}\Big) \\
&\qquad + \left\{ \frac{h}{2} \frac{\partial (\tau_{\alpha\beta}^+ - \tau_{\alpha\beta}^-)}{\partial t} t_\alpha n_\alpha + (\tau_{\alpha 3}^+ + \tau_{\alpha 3}^-) n_\alpha + \frac{h}{2} (\tau_{\alpha\beta,\beta}^+ - \tau_{\alpha\beta,\beta}^-) n_\alpha \right\} \delta w \, dS.
\end{aligned} \tag{A.7}$$

Finally, the boundary conditions of the bulk and surface layers are assembled to give

$$\begin{aligned}
\delta U^{\text{boundary}} &= \int_{\partial S} (N_{\alpha\beta} + \tau_{\alpha\beta}^+ - \tau_{\alpha\beta}^-) n_\beta \, \delta u_\alpha^0 - \Big(M_{\alpha\beta} + \frac{h}{2} (\tau_{\alpha\beta}^+ - \tau_{\alpha\beta}^-) \Big) n_\beta n_\alpha \, \delta\Big(\frac{\partial w}{\partial n}\Big) \\
&\quad + \left\{ \left(\frac{\partial M_{\alpha\beta}}{\partial t} + \frac{h}{2} \frac{\partial (\tau_{\alpha\beta}^+ - \tau_{\alpha\beta}^-)}{\partial t} \right) t_\beta + M_{\alpha\beta,\beta} + \frac{h}{2} (\tau_{\alpha\beta,\beta}^+ - \tau_{\alpha\beta,\beta}^-) + (\tau_{\alpha 3}^+ + \tau_{\alpha 3}^-) \right\} n_\alpha \, \delta w \, dS.
\end{aligned} \tag{A.8}$$

From (A.1), the following equilibrium equations can be obtained:

$$\begin{aligned}
N_{\alpha\beta,\beta} + \tau_{\alpha\beta,\beta}^+ + \tau_{\alpha\beta,\beta}^- + p_\alpha &= 0, \\
M_{\alpha\beta,\alpha\beta} + \frac{h}{2} (\tau_{\alpha\beta,\alpha\beta}^+ - \tau_{\alpha\beta,\alpha\beta}^-) + (\tau_{\alpha 3,\alpha}^+ + \tau_{\alpha 3,\alpha}^-) + p_3 &= 0.
\end{aligned} \tag{A.9}$$

If we set $N^*_{\alpha\beta} = N_{\alpha\beta} + \tau^+_{\alpha\beta} + \tau^-_{\alpha\beta}$ and $M^*_{\alpha\beta} = M_{\alpha\beta} + \frac{h}{2}(\tau^+_{\alpha\beta} + \tau^-_{\alpha\beta})$, (A.9) can be simplified as

$$N^*_{\alpha\beta,\beta} + p_\alpha = 0, \qquad M^*_{\alpha\beta,\alpha\beta} + (\tau^+_{\alpha 3,\alpha} + \tau^-_{\alpha 3,\alpha}) + p_3 = 0. \tag{A.10}$$

This leads to the following possibilities for the boundary conditions:

- u^0_α prescribed or $N^*_{\alpha\beta} n_\beta$ specified.
- $\dfrac{\partial w}{\partial n}$ prescribed or $M^*_{\alpha\beta} n_\alpha n_\beta$ specified.
- w prescribed or $\dfrac{\partial (M^*_{\alpha\beta} t_\beta)}{\partial t} + M^*_{\alpha\beta,\beta} + (\tau^+_{\alpha 3} + \tau^-_{\alpha 3})$ specified.

References

[Abbas and Thomas 1977] B. A. H. Abbas and J. Thomas, "Static stability of plates using fully conforming element", *Int. J. Numer. Methods Eng.* **11**:6 (1977), 995–1003.

[Cammarata 1994] R. C. Cammarata, "Surface and interface stress effects in thin films", *Prog. Surf. Sci* **46**:1 (1994), 1–38.

[Cammarata and Sieradzki 1989] R. C. Cammarata and K. Sieradzki, "Effects of surface stress on the elastic moduli of thin films and superlattices", *Phys. Rev. Lett.* **62**:17 (1989), 2005–2008.

[Cao and Chen 2008] G. Cao and X. Chen, "Size dependence and orientation dependence of elastic properties of ZnO nanofilms", *Int. J. Solids Struct.* **45**:13 (2008), 3821–3844.

[Cho and Parmerter 1994] M. Cho and R. Parmerter, "Finite element for composite plate bending based on efficient higher order theory", *AIAA J.* **32**:11 (1994), 2241–2248.

[Cuenot et al. 2004] S. Cuenot, C. Frétigny, S. Demoustier-Champagne, and B. Nysten, "Surface tension effect on the mechanical properties of nanomaterials measured by atomic force microscopy", *Phys. Rev. B* **69**:16 (2004), 165410.

[Dingreville et al. 2005] R. Dingreville, J. Qu, and M. Cherkaoui, "Surface free energy and its effect on the elastic behavior of nano-sized particles, wires and films", *J. Mech. Phys. Solids* **53**:8 (2005), 1827–1854.

[Gao et al. 2006] W. Gao, S. Yu, and G. Huang, "Finite element characterization of the size-dependent mechanical behaviour in nanosystems", *Nanotechnology* **17**:4 (2006), 1118–1122.

[Gurtin and Murdoch 1975a] M. E. Gurtin and A. I. Murdoch, "Addenda to our paper: a continuum theory of elastic material surfaces", *Arch. Ration. Mech. An.* **59**:4 (1975), 389–390.

[Gurtin and Murdoch 1975b] M. E. Gurtin and A. I. Murdoch, "A continuum theory of elastic material surfaces", *Arch. Ration. Mech. An.* **57**:4 (1975), 291–323.

[Gurtin and Murdoch 1978] M. E. Gurtin and A. I. Murdoch, "Surface stress in solids", *Int. J. Solids Struct.* **14**:6 (1978), 431–440.

[Haiss 2001] W. Haiss, "Surface stress of clean and adsorbate-covered solids", *Rep. Prog. Phys.* **64**:5 (2001), 591–648.

[LAMMPS 2008] S. Plimpton, P. Crozier, and A. Thompson, "LAMMPS: large-scale atomic/molecular massively parallel simulator", Sandia National Laboratories, 2008, Available at http://lammps.sandia.gov.

[Lang et al. 2006] X. Y. Lang, Y. F. Zhu, and Q. Jiang, "Size and interface effects on several kinetic and thermodynamic properties of polymer thin films", *Thin Solid Films* **515**:4 (2006), 2765–2770.

[Liang et al. 2005] H. Liang, M. Upmanyu, and H. Huang, "Size-dependent elasticity of nanowires: nonlinear effects", *Phys. Rev. B* **71**:24 (2005), 241403.

[Lim and He 2004] C. W. Lim and L. H. He, "Size-dependent nonlinear response of thin elastic films with nano-scale thickness", *Int. J. Mech. Sci.* **46**:11 (2004), 1715–1726.

[Lu et al. 2006] P. Lu, L. H. He, H. P. Lee, and C. Lu, "Thin plate theory including surface effects", *Int. J. Solids Struct.* **43**:16 (2006), 4631–4647.

[Miller and Shenoy 2000] R. E. Miller and V. B. Shenoy, "Size-dependent elastic properties of nanosized structural elements", *Nanotechnology* **11**:3 (2000), 139–147.

[Murdoch 1976] A. I. Murdoch, "A thermodynamical theory of elastic material interfaces", *Q. J. Mech. Appl. Math.* **29**:3 (1976), 245–275.

[Oh and Cho 2004] J. Oh and M. Cho, "A finite element based on cubic zig-zag plate theory for the prediction of thermo-electric-mechanical behaviors", *Int. J. Solids Struct.* **41**:5–6 (2004), 1357–1375.

[Oh et al. 2008] J. Oh, M. Cho, and J.-S. Kim, "Buckling analysis of a composite shell with multiple delaminations based on a higher order zig-zag theory", *Finite Elem. Anal. Des.* **44**:11 (2008), 675–685.

[Park and Klein 2008] H. S. Park and P. A. Klein, "Surface stress effects on the resonant properties of metal nanowires: the importance of finite deformation kinematics and the impact of the residual surface stress", *J. Mech. Phys. Solids* **56**:11 (2008), 3144–3166.

[Park et al. 2005] S. H. Park, J. S. Kim, J. H. Park, J. S. Lee, Y. K. Choi, and O. M. Kwon, "Molecular dynamics study on size-dependent elastic properties of silicon nanocantilevers", *Thin Solid Films* **492**:1–2 (2005), 285–289.

[Park et al. 2006] H. S. Park, P. A. Klein, and G. J. Wagner, "A surface Cauchy–Born model for nanoscale naterials", *Int. J. Numer. Methods Eng.* **68**:10 (2006), 1072–1095.

[Pathak and Shenoy 2005] S. Pathak and V. B. Shenoy, "Size dependence of thermal expansion of nanostructures", *Phys. Rev. B* **72**:11 (2005), 113404.

[Shackelford and Alexander 2000] J. F. Shackelford and W. Alexander (editors), *CRC materials science and engineering handbook*, 3rd ed., CRC Press, Boca Raton, FL, 2000.

[Shenoy 2005] V. B. Shenoy, "Atomistic calculations of elastic properties of metallic fcc crystal surfaces", *Phys. Rev. B* **71**:9 (2005), 094104.

[Simmons and Wang 1971] G. Simmons and H. Wang, *Single crystal elastic constants and calculated aggregate properties: a handbook*, MIT Press, Cambridge, MA, 1971.

[Song and Huang 2009] F. Song and G. L. Huang, "Modeling of surface stress effects on bending behavior of nanowires: incremental deformation theory", *Phys. Lett. A* **373**:43 (2009), 3969–3973.

[Song et al. 2010] F. Song, G. L. Huang, and V. K. Varadan, "Study of wave propagation in nanowires with surface effects by using a high-order continuum theory", *Acta Mech.* **209**:1–2 (2010), 129–139.

[Specht 1988] B. Specht, "Modified shape functions for the three-node plate bending element passing the patch test", *Int. J. Numer. Methods Eng.* **26**:3 (1988), 705–715.

[Tsai and Hahn 1980] S. W. Tsai and H. T. Hahn, *Introduction to composite materials*, Technomic, Lancaster, PA, 1980.

Received 5 Jul 2009. Revised 8 Oct 2009. Accepted 16 Oct 2009.

JINBOK CHOI: jbchoi95@snu.ac.kr
WCU Program of Multiscale Mechanical Design, School of Mechanical and Aerospace Engineering, Seoul National University, San56-1, Shillim-dong, Kwanak-gu, Seoul 151-742, Republic of Korea

MAENGHYO CHO: mhcho@snu.ac.kr
WCU Program of Multiscale Mechanical Design, School of Mechanical and Aerospace Engineering, Seoul National University, San56-1, Shillim-dong, Kwanak-gu, Seoul 151-742, Republic of Korea

WONBAE KIM: wbkim@snu.ac.kr
WCU Program of Multiscale Mechanical Design, School of Mechanical and Aerospace Engineering, Seoul National University, San56-1, Shillim-dong, Kwanak-gu, Seoul 151-742, Republic of Korea